

Two-dimensional droplet spreading over random topographical substrates

Nikos Savva,¹ Serafim Kalliadasis,¹ and Grigorios A. Pavliotis²

¹*Department of Chemical Engineering,
Imperial College London, London SW7 2AZ, UK*

²*Department of Mathematics, Imperial College London, London SW7 2AZ, UK*

(Dated: October 7, 2018)

Abstract

We examine theoretically the effects of random topographical substrates on the motion of two-dimensional droplets via appropriate statistical approaches. Different random substrate families are represented as stationary random functions. The variance of the droplet shift at both early times and in the long-time limit is deduced and the droplet footprint is found to be a normal random variable at all times. It is shown that substrate roughness decreases droplet wetting, illustrating also the tendency of the droplet to slide without spreading as equilibrium is approached. Our theoretical predictions are verified by numerical experiments.

PACS numbers: 05.10.Gg, 47.15.gm, 47.55.D-, 68.08.Bc

Front propagation in heterogeneous media occurs in a wide variety of areas in physics, ranging from transport phenomena in porous media and reaction-diffusion-advection systems to crack propagation due to lattice defects [1]. Heterogeneities are always present in natural environments but quite often their precise form is unknown. In such cases they can be modeled as random noise signals, a more physical and practical assumption than e.g. periodic ones. An example of front propagation central to interfacial hydrodynamics is that of a moving contact line during liquid spreading on a solid substrate, where heterogeneities usually originate from substrate defects, either chemical [2] or topographical [3].

It is a fundamental problem to understand how random heterogeneities influence the spreading dynamics and the characteristics of contact line propagation, e.g. speed and location. Experimental studies on droplet spreading – a simple prototype for the study of contact line motion – suggest that substrates having highly irregular micro-scale features, commonly called rough, can influence the dynamics significantly [4]. Several theoretical works focused on equilibrium configurations and deterministic substrates: the study by Wenzel [5] on droplet equilibria on rough substrates obtained an effective contact angle based on simplistic energy arguments – a formula which was supported by experiments in a regime where the contact angles are not small [3]; in [6] the contact line of a fluid wedge in the presence of a single, localized defect was determined; in [7] droplet equilibria on substrates with regular, periodic features were considered; Cox [8] investigated multiple equilibria of an infinite fluid wedge on a general non-periodic rough surface. Introducing randomness in the variations of the substrates is clearly a realistic way to represent roughness. There are a few studies in this direction but are based on phenomenological modeling ideas as for example [9] which regarded rough substrate patches as contact angle point sources or [10] which looked into the effects of surface roughness using an Ising model. Studies on contact line dynamics on random substrates were also based on phenomenological ideas, e.g. [11] where postulated equations describing the dynamics were utilized. Hence, to date a systematic fluid dynamics treatment based on rational statistical approaches is still lacking. As a result, contact line motion on heterogeneous substrates is far from being well understood, unlike other problems in continuum mechanics, such as porous media, which not only have been analyzed from first principles but have also motivated new mathematical approaches (cf. homogenization [12]).

In this Letter we report the first detailed and systematic study of the qualitative effects of random, small-scale spatial heterogeneities on droplet motion, through the development

of appropriate statistical methodologies. The starting point is the recent work in [13] on the motion of two-dimensional (2D), partially wetting droplets over deterministic, spatially heterogeneous substrates. The restriction to 2D implies that there are no transverse variations and the contact line is essentially treated as a set of two points. This simplified problem, albeit more difficult to study experimentally, is a first step towards understanding the influence of spatial heterogeneities, but the required analysis still remains highly nontrivial. The model for the droplet motion was obtained rigorously from the governing hydrodynamic equations. Assuming small contact angles, a long-wave expansion in the Stokes flow regime, yields a single equation for the evolution of the droplet thickness $H(x, t)$ over a substrate $\eta(x)$. In dimensionless form the equation reads:

$$\partial_t H + \partial_x [H^2 (H + \lambda) \partial_x^3 (H + \eta)] = 0, \quad (1)$$

where $\lambda \ll 1$ is the non-dimensional slip length originating from the Navier model imposed to alleviate the stress singularity that occurs at the moving contact line [14]. Equation (1) describes the capillarity driven spreading that is resisted by fluid viscosity: the term $\partial_t H$ results from the viscous fluid motion and the term $\partial_x[\cdot]$ represents the effect of surface tension and also accounts for the substrate curvature which contributes an additional capillary pressure, $-\partial_x^2 \eta$. The spatial coordinate x , and time t , are made non-dimensional by the characteristic length $L = \sqrt{A/(2\alpha_s)}$ and time $\tau = 3\mu L/(\gamma\alpha_s^3)$, respectively, where A is the droplet cross-sectional area, α_s is the equilibrium angle prescribed by Young's law, μ is the viscosity and γ is the surface tension. $\eta(x)$ and $H(x)$ are scaled by $L\alpha_s$ and λ by $L\alpha_s/3$ respectively. Equation (1) is subject to a constant volume constraint and the boundary conditions at the contact points that the droplet thickness vanishes and the angle the free surface makes with the substrate remains equal to its static value, α_s . For quasi-static spreading, a singular perturbation method was employed in [13] to asymptotically match the solution in the bulk of the fluid with the solution in the vicinity of the contact lines. This led to a set of two integro-differential equations (IDEs) for the time-evolution of the right and left contact points at $x = a_{\pm}(t)$, respectively. Their validity has been confirmed by comparisons with numerical solutions to the full equation in (1) [13].

Here we use the set of IDEs to investigate the case where $\eta(x)$ is a random function. We take $|\eta(x)| \ll 1$ assuming also that its variations occur at lengthscales that are much longer than λ . The requirement of substrate smoothness together with the fact that the ‘noise’

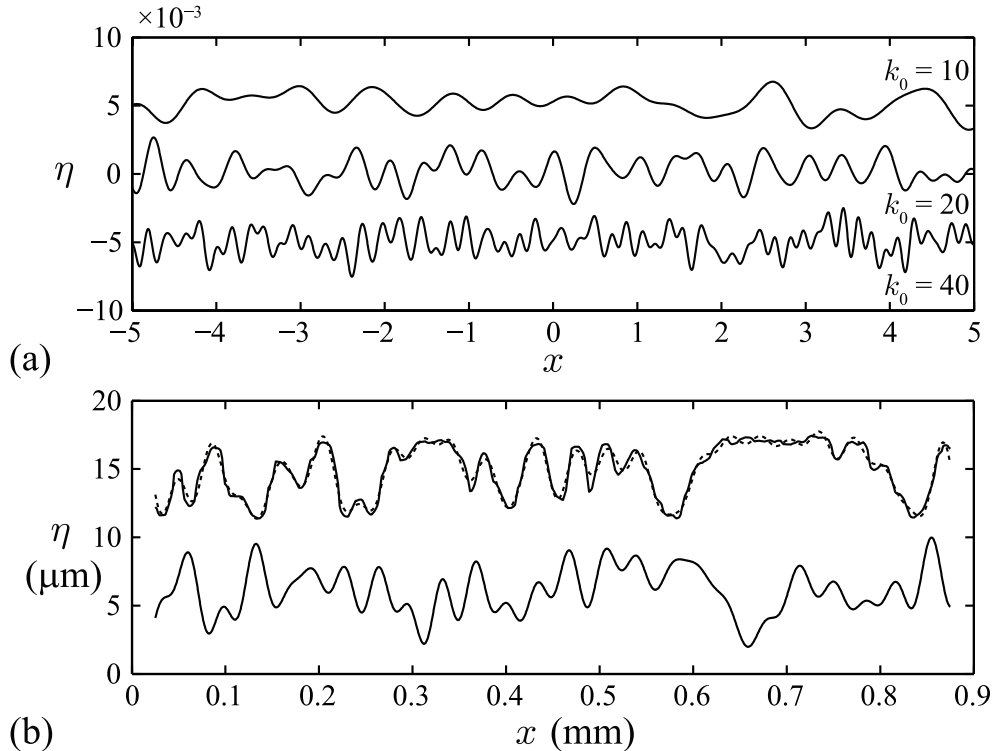


FIG. 1: (a) Sample substrate realizations using (2) for $\eta_0 = 10^{-3}$ and $k_0 = 10, 20$ and 40 . (b) Top plot. Solid line: experimental profile from Hitchcock *et al.* [3] for an alumina sample. Dashed line: approximation obtained by projecting the experimental profile onto $N = 26$ harmonics in (2). Lower plot: sample substrate realization for the same η_0 and k_0 , but $N = 1000$.

is spatial and enters the equations in a nonlinear fashion, precludes casting the problem into the standard Langevin-Fokker-Planck formalism, which is usually employed to study randomly perturbed dynamical systems [15].

The primary fundamental difficulty with the substrate is the development of a random representation that can have a large frequency content and at the same time it is differentiable. A convenient representation is the random function,

$$\eta(x) = \frac{\eta_0}{\sqrt{N}} \sum_{m=1}^N \alpha_m \sin \frac{k_0 m}{N} x + \beta_m \cos \frac{k_0 m}{N} x, \quad (2)$$

where $\eta_0 \ll 1$ and k_0 are the characteristic amplitude and wavenumber of the substrate, respectively, and N is a large positive integer. Here the coefficients α_m and β_m are statistically independent normal variables with unit variance. It is readily seen that $\eta(x)$ is a periodic function with period $2\pi N/k_0$, but we eventually take $N \rightarrow \infty$ so that this periodicity is

lost and $\eta(x)$ approaches a band-limited white noise (see Fig. 1a; in this limit, continuity of (2) and all its derivatives can be carefully shown by Kolmogorov’s continuity theorem). Representations of this form, are also invoked to look into noise effects in other contexts as they occur, for example, in electrical current signals or in black-body radiation [16].

An attractive feature of the stochastic representation in (2) is that it generates an infinite family of substrate realizations parameterized by two parameters, η_0 and k_0 , which are often reported in experimental studies when characterizing a rough substrate (in Fig. 1b, $\eta_0 \sim 0.78 - 2.1\mu\text{m}$, wavelength $l_0 \sim 14 - 42\mu\text{m}$). These two parameters may be also be used to compute the ‘roughness coefficient of the substrate’, r , defined as the mean of the ratio of the actual surface area over its projected area. In the limit of $\eta_0 k_0 \ll 1$ we find $r = 1 + \eta_0^2 k_0^2 / 6$, to be contrasted with $r = 1 + \eta_0^2 k_0^2 / 4$ obtained with the pure harmonic $\eta(x) = \eta_0 \cos k_0 x$ [17]. Comparison with experimental substrate profiles determined by Hitchcock *et al.* [3] shows that (2) can be used to realistically represent actual rough substrates. For example, given the experimental profile in Fig. 1b (solid line of the upper plots), k_0 is readily determined from $k_0 = 2\pi n / \sqrt{5/3}$ and η_0 from $\eta_0 = \sqrt{\langle \eta^2 \rangle}$, where n corresponds to the number of maxima per unit length [16] and $\langle \cdot \rangle$ denotes an ensemble average over all substrate realizations. To obtain the dashed profile as an approximation to the experimental profile using (2), the finite length of the profile is matched to the period of (2) to get $N = 26$, which then allows us to determine the α_m and β_m by projecting the experimental profile onto their corresponding harmonics. On the other hand, the lower plot in Fig. 1b is generated with random α_m and β_m with $N = 1000$, where η_0 and k_0 are kept the same so that the lower plot belongs to the same substrate family with the upper one. For the statistical analysis that follows, a large number of substrate realizations, typically 20,000, will be utilized.

Different substrate descriptions might have been used that have been observed in profilometry measurements, as for example representations that exhibit statistical self-affinity, whose spectral density follows the power law $\propto k^{2D-5}$ [20], where $1 < D < 2$ is the fractal dimension. The differentiability requirement of the substrate representation together with the fact that in reality a self-affine structure cannot persist for all lengthscales requires imposing lower and upper wavenumber cutoffs. However, as we shall see later the results for the statistics of the contact line motion are qualitatively the same regardless of the representation we employ.

To facilitate the analysis, we introduce the *contact line fluctuation* ε and *droplet shift* ℓ

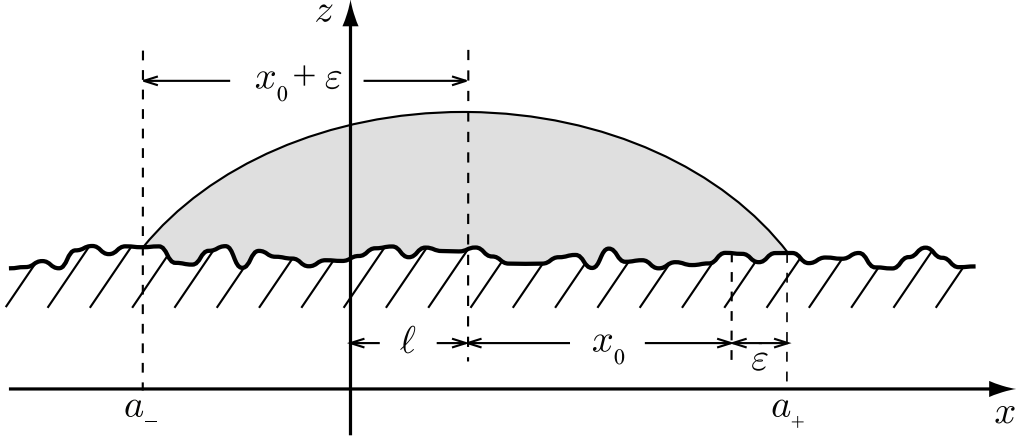


FIG. 2: Droplet lying between $a_- \leq x \leq a_+$ on a random topographical substrate. The droplet shift, $\ell = \frac{1}{2}(a_+ + a_-)$, is the distance the droplet midpoint moves away from $x = 0$ and the contact line fluctuation, $\varepsilon = \frac{1}{2}(a_+ - a_-) - x_0$, measures deviations of the contact line location away from the flat-substrate radius, $x_0(t)$.

along the substrate (see Fig. 2), defined in terms of the contact line locations as

$$\varepsilon = \frac{1}{2}(a_+ - a_-) - x_0 \quad \text{and} \quad \ell = \frac{1}{2}(a_+ + a_-), \quad (3)$$

where x_0 is the contact line location when the droplet spreads on a flat substrate symmetrically about $x = 0$, which approaches $\sqrt{3}$ in the long time limit. The droplet shift is a measure of the distance the droplet midpoint is displaced from $x = 0$, whereas the contact line fluctuation measures the deviation of the droplet radius from the flat-substrate radius. As the amplitude of the topographical features is taken to be small, we also expect $\varepsilon \ll 1$. By linearizing about the flat-substrate equilibrium we obtain

$$\varepsilon = \frac{3\eta_0}{2\sqrt{N}} \sum_{m=1}^N (\alpha_m \sin \lambda_m \ell + \beta_m \cos \lambda_m \ell) \mathcal{I}(\sqrt{3}\lambda_m), \quad (4)$$

$$\sum_{m=1}^N (\alpha_m \cos \lambda_m \ell - \beta_m \sin \lambda_m \ell) \mathcal{J}(\sqrt{3}\lambda_m) = 0, \quad (5)$$

where $\lambda_m = k_0 m/N$, $\mathcal{I}(x) = \text{sinc } x - \cos x - (x/3) \sin x$ with $\text{sinc } x = x^{-1} \sin x$ and $\mathcal{J}(x) = x \cos x - \sin x$. By looking at the neglected terms in this linearization procedure, we find that (4) and (5) accurately predict droplet equilibria provided that $\eta_0 k_0^2 \ll 1$. To conform with this condition, together with our principal aim to examine the effects of small scale roughness, we focus on substrate families with $\eta_0 \ll 1$ and $1 \ll k_0 \ll \eta_0^{-1/2}$. Hence, for

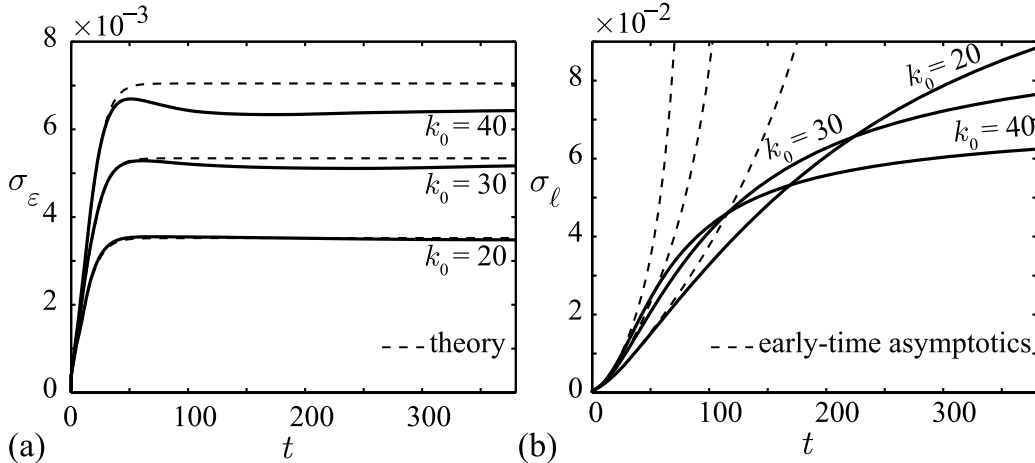


FIG. 3: Dynamics of droplet spreading over randomly varying substrates with $\eta_0 = 5 \times 10^{-4}$ and $k_0 = 20, 30$ and 40 using 20,000 samples for each substrate family. (a) Standard deviation of ε as a function of time. The numerical experiments (solid line) are indistinguishable from theory (dashed line) for $k_0 = 20$. (b) Standard deviation of ℓ as a function of time. The early-time asymptotics agree with numerical experiments up to $t \sim \mathcal{O}(30)$. For large times the solid lines asymptote at values predicted from the long-time analysis.

a droplet with $L = 0.5\text{mm}$, $\alpha_s = 15^\circ$ and substrate topographies with amplitudes $0.5\mu\text{m}$ ($\eta_0 \approx 4 \times 10^{-4}$), $\eta_0 k_0^2 < 1$ for $l_0 > 77\mu\text{m}$ (beyond the region of wavelengths in Fig. 1b, but Hitchcock *et al.* give materials with smaller amplitudes and larger wavelengths, e.g. for silica, $\eta_0 \sim 0.006 - 3.1\mu\text{m}$, $l_0 \sim 65 - 110\mu\text{m}$). At these scales, slip is more important than intermolecular forces in controlling the spreading dynamics, as the study by Hocking on droplet spreading over flat substrates has demonstrated [18]. By the central limit theorem, we also see from (4) that ε is approximately a normally distributed random variable. Contributions to its mean are of $\mathcal{O}(\eta_0)$ and originate from $\langle \alpha_m \sin \lambda_m \ell + \beta_m \cos \lambda_m \ell \rangle$. If all equilibria are taken into account however, this quantity vanishes and contributions to the mean are of $\mathcal{O}(\eta_0^2)$. Therefore, to fully assess the effects of spatial heterogeneities on wetting, the equilibria attained from the droplet dynamics need to be considered instead.

For arbitrary t , the IDEs obtained for deterministic substrates in [13] are appropriately modified to model random spatial heterogeneities described by (2) and are linearized for

$\varepsilon \ll 1$. This calculation is rather involved and lengthy. The final equations are of the form,

$$\begin{aligned}\dot{\varepsilon} + \mathcal{A}(t) \varepsilon &= \frac{\eta_0}{\sqrt{N}} \sum_{m=1}^N (\alpha_m \sin k_m \ell + \beta_m \cos k_m \ell) \mathcal{B}(t, k_m), \\ \dot{\ell} &= \frac{\eta_0}{\sqrt{N}} \sum_{m=1}^N (\alpha_m \cos k_m \ell - \beta_m \sin k_m \ell) \mathcal{C}(t, k_m),\end{aligned}$$

where $\mathcal{A}(t)$, $\mathcal{B}(t, k_m)$ and $\mathcal{C}(t, k_m)$ are complicated functions of their arguments that we omit here for the sake of brevity. Their time-dependence enters through x_0 and its time derivative with x_0 satisfying, $3x_0 \ln[2x_0/(\lambda e^2)] = 27x_0^{-6} - 1$. The linearity of the equation for ε also implies that this quantity is a normal variable for all times, whose variance may be computed explicitly. Figure 3a shows plots of the standard deviation of ε , σ_ε , as a function of time for $\eta_0 = 5 \times 10^{-4}$ and $k_0 = 20, 30$ and 40 . When $k_0 = 20$, the theoretically predicted curve is indistinguishable from the one obtained from numerical experiments, but as expected the agreement tends to degrade as the condition $\eta_0 k_0^2 \ll 1$ no longer holds. Determining the time-evolution of the standard deviation of ℓ , σ_ℓ , explicitly is a formidable task due to the highly non-linear nature of the equation for ℓ , but the early-time behavior can be found by linearizing about $\ell = 0$. In Fig. 3b we show the evolution of σ_ℓ as computed from numerical experiments, together with the early-time behavior predicted by the linear theory for the same parameters as in Fig. 5b. There is excellent agreement up to $t \sim \mathcal{O}(30)$; after that time the theoretically predicted variance goes to infinity since the linearized equation for ℓ predicts a Cauchy variable in the long-time limit. Comparing the time-scales over which σ_ε and σ_ℓ saturate, reveals that the droplet ‘footprint’, $2(\varepsilon + x_0)$, approaches equilibrium over a shorter timescale compared to the time for ℓ to reach equilibrium, which suggests that the droplet slides without spreading along the various substrate features to find the final equilibrium position.

In the long-time limit, we cannot solve for ℓ explicitly since (5) is nonlinear and moreover it admits infinitely many solutions. However, the evolution towards equilibrium fixes the solution to (5) to be the stable equilibrium that is closest to $\ell = 0$, a problem which is reminiscent of the highly nontrivial ‘first-passage problem’ in probability theory [16]. Interestingly, Fig. 4a reveals that the probability density of ℓ as $t \rightarrow \infty$, p_ℓ , is far from being a normally distributed random variable as the comparison with the density of the normal variable with the same variance demonstrates. By taking into account the mean distance between zeros of (5) [16], together with the fact that on average half of the closest equilibria

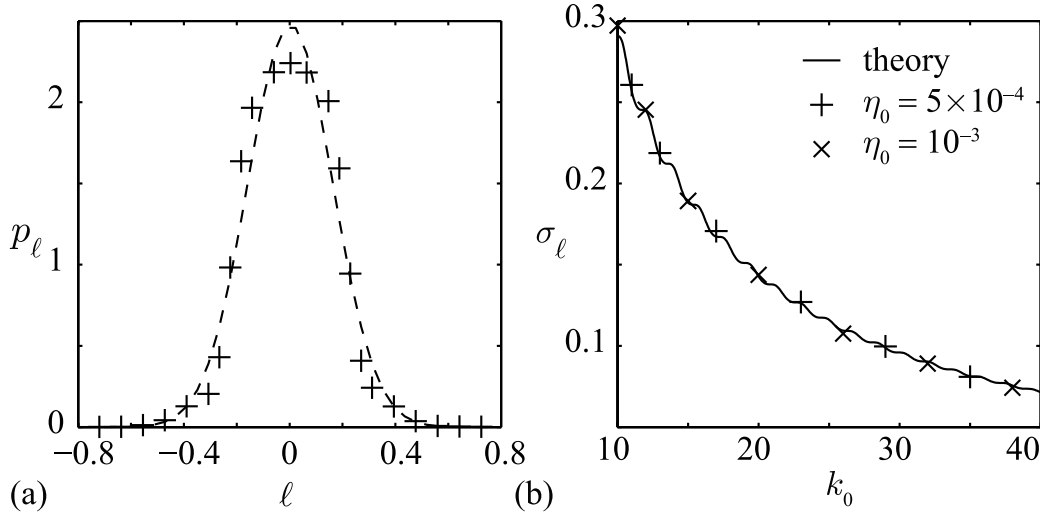


FIG. 4: Statistics of ℓ for k_0 ranging from 10 to 40 with $\eta_0 = 5 \times 10^{-4}$, (+) and 10^{-3} , (x), taken over 20,000 samples and $N = 1,000$. (a) Probability density function of ℓ when $\eta_0 = 5 \times 10^{-4}$ and $k_0 = 20$ compared with a normal density of the same variance (dashed line); (b) Standard deviation of ℓ as a function of k_0 , illustrating the excellent agreement of (6) with numerics.

are unstable, we find that

$$\sigma_\ell^2 = \frac{5}{6}\pi^2 k_0^{-2} \left(1 - \frac{1}{2} \text{sinc } 2\sqrt{3}k_0\right) + \mathcal{O}(k_0^{-4}) \quad (6)$$

in the limit $k_0 \gg 1$. It is clear that as the substrate features become rougher the droplet has a tendency to shift/slide less along the substrate. This behavior is confirmed in Fig. 4b, where we plot the theoretically predicted σ_ℓ as a function of k_0 together with numerical experiments for different substrate families, confirming also the independence of ℓ on η_0 .

From our numerical experiments we also found that $\langle \varepsilon \rangle < 0$ in the long-time limit, thus suggesting that surface roughness reduces wetting. Such behavior appears to contradict Wenzel's theory but it signifies the fact that the droplet has to overcome the energy barriers that separate the multiple equilibrium droplet states. This effect is demonstrated in the recent experiments of Chung *et al* [19], where spreading perpendicular to the grooves of parallel-grooved substrates violates Wenzel's law, and further supported by the work of Cox [8] on wedge equilibria over (deterministic) three-dimensional rough substrates, who postulated that roughness-induced wetting enhancement is due to a higher-order effect which manifests itself when spreading does not occur perpendicular to the substrate grooves. A semi-analytical expression for $\langle \varepsilon \rangle$ can be obtained by noting that from our numerical exper-

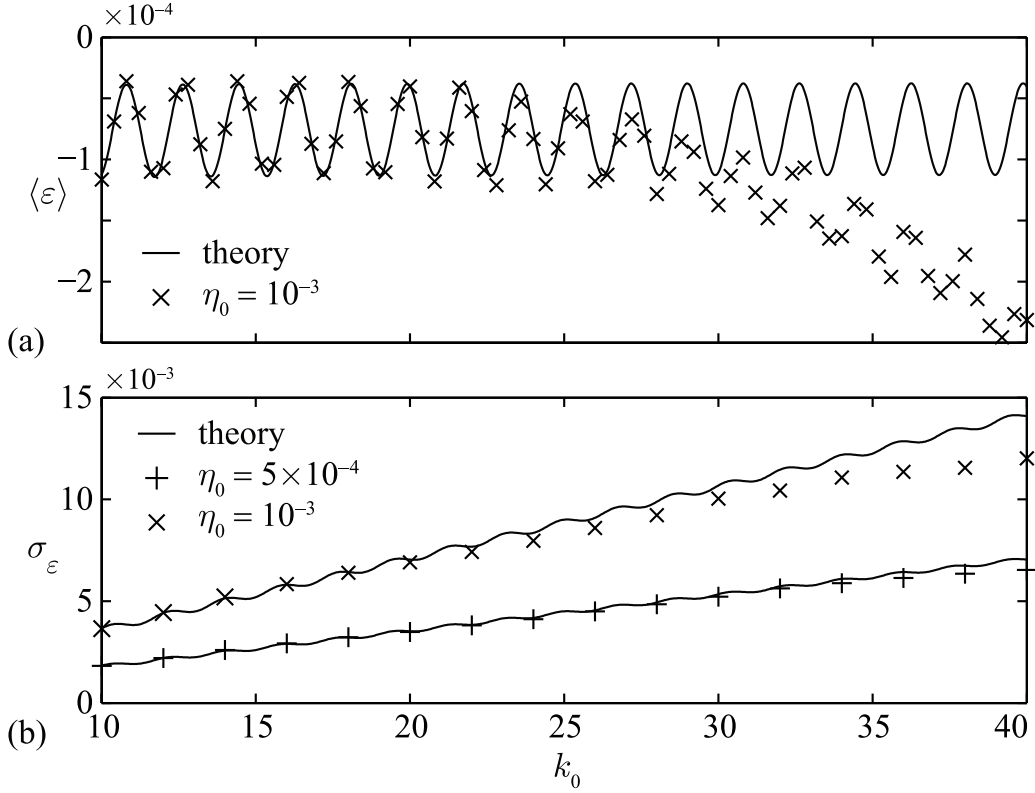


FIG. 5: Statistics of ε for the same parameters as in Fig. 4. (a) Comparison of the numerically determined $\langle\varepsilon\rangle$ and $\langle\varepsilon\rangle_{\text{approx}}$ as a function of k_0 ; (b) Comparison of the theoretical and numerical standard deviation of ε as a function of k_0 . The agreement is excellent for $\eta_0 k_0^2 \ll 1$.

iments, $\langle\alpha_m \sin \lambda_m \ell + \beta_m \cos \lambda_m \ell\rangle = F(k_0) \mathcal{J}(\sqrt{3}\lambda_m)/(k_0\sqrt{3})$, where F appears to depend weakly on η_0 and k_0 and equals to 3 for $\eta_0 k_0^2 \ll 1$. Based on this observation, $\langle\varepsilon\rangle$ is found to be

$$\langle\varepsilon\rangle_{\text{approx}} \approx -\frac{3}{8}\eta_0 \left(2 - \cos 2\sqrt{3}k_0\right) + \mathcal{O}(\eta_0 k_0^{-1}), \quad (7)$$

suggesting that $\langle\varepsilon\rangle$ has an oscillatory behavior as k_0 varies. Furthermore, the mean apparent contact angle is now larger than the static contact angle by an amount $2|\langle\varepsilon\rangle|/\sqrt{3}$ to leading order in ε . Figure 5a depicts a plot of (7) as a function of k_0 together with the mean obtained in numerical simulations for substrates with $\eta_0 = 10^{-3}$, considering 20,000 samples from each substrate family. For smaller k_0 , the agreement between the semi-analytic approximation and the numerical experiments is evident, but as the substrate becomes more rough so that $\eta_0 k_0^2 \ll 1$ is no longer valid and nonlinear effects become appreciable, there is a clear deviation towards a progressive reduction of the mean droplet radius. This implies that the

apparent contact angle tends to increase with substrate roughness, thus pointing towards a substrate-induced, hysteresis-like effect.

The variance of ε can be deduced from (4) by converting the Riemann sum into an integral by taking $N \rightarrow \infty$,

$$\sigma_\varepsilon^2 = \frac{1}{8}\eta_0^2 k_0^2 \left(1 - 3 \operatorname{sinc} 2\sqrt{3}k_0\right) + \mathcal{O}(\eta_0^2), \quad (8)$$

when $k_0 \gg 1$. The theoretically predicted σ_ε is in very good agreement with the simulated one as shown in Fig. 5b, where we plot σ_ε as a function of k_0 when $\eta_0 = 5 \times 10^{-4}$ and $\eta_0 = 10^{-3}$. Had we used a self-affine substrate representation, the results are qualitatively the same since the leading order variance of ε differs from the leading order of (8) only by a factor $3(2 - D)(g^{4-2D} - g^2)/[(D - 1)(1 - g^{4-2D})]$, that depends on two additional parameters, namely the fractal dimension D and on the lower to upper cutoff wavenumber ratio, g . Numerical studies of σ_ℓ also confirm qualitative agreement.

To conclude, we have presented the first detailed and systematic investigation of the motion of 2D droplet fronts over randomly varying shallow substrates by using a model derived first principles, i.e. from the governing hydrodynamic equations in the limit of small contact angles. Analytical predictions made for the equilibria of the two quantities of interest, the contact line fluctuation ε and droplet shift along the substrate ℓ exhibit excellent agreement with numerical experiments. However, our analysis revealed that considering droplet equilibria alone cannot fully determine the effects of random substrates on wetting; instead, their stability from the dynamical spreading problem needs to be taken into account as well. For arbitrary times, examination of the evolution of ℓ and ε suggests that on average the droplet has the tendency to slide without spreading along the substrate before reaching equilibrium. In the long-time limit, ℓ and ε scale with $\sigma_\varepsilon^2 \sim \eta_0^2 k_0^2 / 8$ and $\sigma_\ell^2 \sim 5\pi^2 k_0^{-2} / 6$, respectively. We believe that these results will motivate further analytical and experimental studies on the role of heterogeneities on wetting hydrodynamics.

We thank the anonymous referee for suggesting the statistical self-affine substrate representation. We acknowledge financial support from EPSRC Platform Grant No. EP/E046029.

-
- [1] G. M. Homsy, *Annu. Rev. Fluid Mech.* **19**, 271 (1987); R. B. Philips, *Crystals, Defects and Microstructures. Modeling Across Scales* (Cambridge University Press, Cambridge, 2001); J.

- Xin, *SIAM Rev.* **42**, 161 (2000).
- [2] L. W. Schwartz and R. R. Elley, *J. Coll. Int. Sci.* **202**, 173 (1998); L. W. Schwartz, *Langmuir* **14**, 3440 (1998); T. Cubaud and M. Fermigier, *J. Coll. Int. Sci.* **264**, 171 (2004).
- [3] S. J. Hitchcock, N. T. Carroll, and M. G. Nicholas, *J. Mater. Sci.* **16**, 714 (1981); S. Shibuichi, T. Onda, N. Satoh, and K. Tsujii, *J. Phys. Chem.* **100**, 19512 (1996); J. Bico, C. Tordeaux, and D. Quéré, *Europhys Lett.* **55**, 214 (2001).
- [4] A. M. Cazabat and M. A. Cohen-Stuart, *J. Phys. Chem.* **90**, 5845 (1986).
- [5] R. N. Wenzel, *Ind. Eng. Chem.* **28**, 988 (1936).
- [6] J. F. Joanny and P.-G. de Gennes, *J. Chem. Phys.* **81**(1), 552 (1984).
- [7] R. E. Johnson and R. H. Dettre, *Adv. Chem. Ser.* **43**, 112 (1964); L. M. Hocking, *J. Fluid Mech.* **76**, 801 (1976); C. Huh and S. G. Mason, *J. Coll. Int. Sci.* **60**, 11 (1977); X. B. Zhou and J. Th. M. De Hosson, *J. Mater. Res.* **10**, 1984 (1995).
- [8] R. G. Cox, *J. Fluid Mech.* **131**, 1 (1983).
- [9] K. M. Jansons, *J. Fluid Mech.* **154**, 1 (1985).
- [10] C. Borgs, J. De Connick, R. Kotecký, and M. Zinque, *Phys. Rev. Lett.* **74**, 2292 (1995).
- [11] S. Mulinet, C. Guthmann, and E. Rolley, *Eur. Phys. J. E* **8**, 437 (2002); A. Tanguy and T. Vettorel, *Eur. Phys. J. B* **38**, 71 (2004).
- [12] G. A. Pavliotis and A. M. Stuart, *Multiscale Methods: Averaging and Homogenization* (Springer, NY, 2008).
- [13] N. Savva and S. Kalliadasis, *Phys. Fluids* **21**, 092102 (2009).
- [14] C. Huh and L. E. Scriven, *J. Coll. Int. Sci.* **35**, 85 (1971).
- [15] C. W. Gardiner, *Handbook of Stochastic Methods* (Springer, Berlin, 1985).
- [16] S. O. Rice, *Bell Sys. Tech. J.* **23**, 282 (1944) and **24**, 46 (1945).
- [17] P.-G. de Gennes, F. Brochard-Wyart and D. Quéré, *Capillarity and Wetting Phenomena* (Springer, NY, 2003).
- [18] L. M. Hocking, *Phys. Fluids* **6**(10), 3224 (1994).
- [19] J. Y. Chung, J. P. Youngblood, and C. M. Stafford, *Soft Matter* **3**, 1163 (2007).
- [20] T. R. Thomas, *Rough Surfaces* (Imperial College Press, London, 1999); A. Majumdar and C. L. Tien, *Wear* **136**, 313 (1990).